OPEN ACCESS

ISSN: 3066-0807

Kaipeng L and Ling W (2026): 1590-1594
Int J Teach Learn Sci, 3(6): 156
DOI: 10.71010/3066-0807/ijtls-e156

Research Article

International Journal of Teaching and Learning Sciences

Lifetime Prediction of Flyback Micro-Inverters Operating in Discontinuous Conduction Mode (DCM)

By Topalis Andreas*

Supervisor: Ganatsios Stergios, Department of Electrical and Computer Engineering, University of Western Macedonia Faculty of Engineering, 50100 Kozani, www.uowm.gr.

***Corresponding author:** Topalis Andreas, Email: satan131984@hotmail.com

Citation: Andreas T (2026) Lifetime Prediction of Flyback Micro-Inverters Operating in Discontinuous Conduction Mode (DCM). Int J Teach Learn Sci: IJTLS-156. 3(6) 1-5.

Received Date: 25 September, 2026; **Accepted Date:** 30 September, 2026; **Published Date:** 05 October, 2026

Abstract

Investigations into micro-inverters, intended for photovoltaic (PV) systems hooked up to the power grid, have seen a surge lately. This is largely attributed to their impressive functionality, particularly when dealing with uneven solar irradiance. Concurrently, it's crucial that a micro-inverter possesses a lifespan at a minimum equal to that of the PV panel it serves, implying an operational duration exceeding two decades. Consequently, assessing the operational lifespan of micro-inverters represents a crucial consideration, largely constrained by the endurance of the semiconductors within the internal circuitry. The longevity of these semiconductors hinges directly upon the average temperature observed at their junctions, alongside the variations in temperature they experience. In single-phase systems, the power delivered fluctuates at double the frequency of the power grid. As a consequence, the power dissipated within the semiconductor components undergoes corresponding oscillations, also occurring at twice the grid's frequency. This fluctuating loss of power then leads to a rise in the average temperature of the semiconductor junctions, coupled with fluctuations in this junction temperature. Prior research indicates that semiconductor lifespan correlates with both the mean junction temperature and the magnitude of the temperature variation, expressed as peak-to-peak swing. Semiconductor thermal behavior varies; consequently, equivalent power dissipation leads to distinct average temperatures and oscillations. Hence, informed selection of a switching configuration demands consideration of dynamic thermal analysis.

This study presents a refined dynamic thermal model specifically developed for computing the junction temperature of the primary switch within a flyback micro-inverter. The subsequent findings indicate the feasibility of employing either the SUU09N10-76P or the IRFI540G MOSFET in the construction. Notably, the IRFI540G exhibits a significantly extended operational lifespan, outperforming the SUU09N10-76P by a factor of 13,000.

Keywords: *Photovoltaics, DCM Flyback micro-inverter, lifetime estimation.*

1. Introduction

There are three primary architectures for grid-tied solar photovoltaic (PV) inverters: central, chain, and micro-inverters. Central inverters, alongside array inverters, tend to suffer from elevated power losses when exposed to shading. Conversely, micro-inverters, specifically designed for individual PV modules, permit each module to function at its optimal power output. This characteristic enhances performance, especially in situations where partial shading is present.

The existing body of research extensively covers micro-inverter architectures [1]. Among these, designs leveraging Discontinuous Conduction Mode (DCM) flyback micro-inverters stand out as particularly appealing. Their advantages lie in straightforward control mechanisms, reduced production costs, and their suitability for modular configurations. However, the inherent operational characteristics of DCM present a drawback: they lead to a considerable rise in the Root Mean Square (RMS) current within the primary circuit, which, in turn, elevates both conduction and switching losses.

A review of existing research reveals a significant body of work dedicated to increasing the lifespan of DCM flyback micro-converters. This includes approaches like eliminating electrolytic capacitors, alongside various modifications to the circuit's fundamental design. Nevertheless, accurately forecasting the operational longevity of these micro-converters presents a distinct challenge. This issue of predicting service life is predominantly governed by the endurance of the semiconductor components utilized within the circuitry.

Microinverters interface with the power grid through a single-phase arrangement. As a direct result of this, the power delivered to the grid pulsates, exhibiting oscillations at a rate that is double the grid's frequency. Because of this, power dissipation and the junction temperature experienced by the semiconductor switches also experience these fluctuations, twice the grid's frequency. Research findings suggest a connection where the lifespan of semiconductors is determined by the average temperature experienced at the junction, along with the overall amplitude, measured peak-to-peak, of the temperature variations. Temperature fluctuations are gauged through the utilization of diverse measurement techniques. Examples of these methods encompass approaches like isoplanar contribution determination, peak enumeration, the rudimentary amplitude/average computation, and rainflow analysis. The point of system malfunction is defined as being reached after a count of N_f oscillations, as empirically established via the aging tests performed.

Within flyback DCM micro-inverters, the primary switch S_1 (depicted in Figure 1) experiences substantial power losses. These losses fluctuate at a frequency double that of the grid, potentially curtailing operational lifespan. Consequently, to guarantee a lengthy service life exceeding 20 years, similar to that of photovoltaic modules, it becomes imperative to conduct a thermal evaluation to facilitate the selection of a suitable switch.

The chosen switch in this study is MOSFET S_1. Section 2 delves into the power losses exhibited by these MOSFETs. Sections 3 and 4 then introduce the thermal model and the methodology for predicting the lifespan of the MOSFETs, respectively. The findings of the investigation are subsequently presented in section 6.

2. Micro-Inverter Flyback Analysis

Operating mode 1: Figure 1 presents a standard circuit schematic for a typical flyback micro-inverter design, complete with a leakage path. This design incorporates three primary switching elements: S_1, S_2, and S_3. Switch S_1 is driven at a high pulse-width modulation (PWM) frequency with the intention of generating a sinusoidal output current waveform. Conversely, switches S_2 and S_3 are synchronized to the grid frequency. The elevated switching frequency employed for S_1, however, introduces substantial switching losses. Furthermore, the primary side root mean square (RMS) current, denoted as ($I_{p,rms}$), is increased by operation in the discontinuous conduction mode (DCM), which, in turn, leads to greater conduction losses.

Consequently, the micro-converter designated S_1 accounts for the most substantial proportion of overall losses within the entire circuit. Due to this, neglecting the dynamic thermal examination during selection could potentially lead to S_1 experiencing the briefest operational lifespan in the system.

To determine the energy lost in S_1, plotting the turn-on and turn-off currents over N switching cycles is the initial step. The conduction currents flowing through S_1 can be visualized as shown in the provided figure 2:

$$i_p(t) = \frac{V}{L_m} t \quad 0 < t \le d_i T_s \quad (1)$$

Let's denote the i-th switching cycle. Furthermore, the duty cycle, which we will represent as d_i, can be expressed as follows:

$$d_i = D_m \left| \sin\left(\frac{\pi}{N} i\right) \right|, 1 \le i \le N \quad (2)$$

The highest possible duty cycle, represented as D_m, is determined by the DC input voltage V_{dc}, the maximum mains voltage V_{gm}, and the rotational speed n.

$$D_m \le \frac{1}{1 + \frac{V_{dc}}{nV_{gm}}} \quad (3)$$

However, in reality, when the gate signal of the switch S_1 is at zero, there are switching losses. This happens because the current doesn't stop immediately, but keeps flowing through S_1 while it's closing over the period denoted as t_f. Supposing the current's reduction follows a straight-line pattern, we can deduce the following:

$$i_p(t) = i_{peak,i} - i_{peak,i}\left(\frac{t - d_i T_s}{t_f}\right) \quad d_i T_s < t \le d_i T_s + t_f \quad (4)$$

Let's denote $i_{peak,i}$ as the peak current of switch S_1 within the i-th switching cycle. Its value can be expressed as follows:

$$i_{peak,i} = \frac{V}{L_m} d_i T_s \quad (5)$$

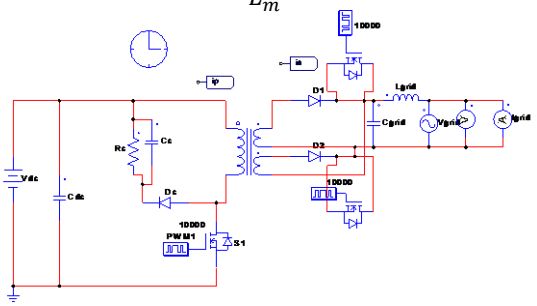


Figure 1: Main geometry of DCM flyback micro-converters by PSIM program (PSIM).

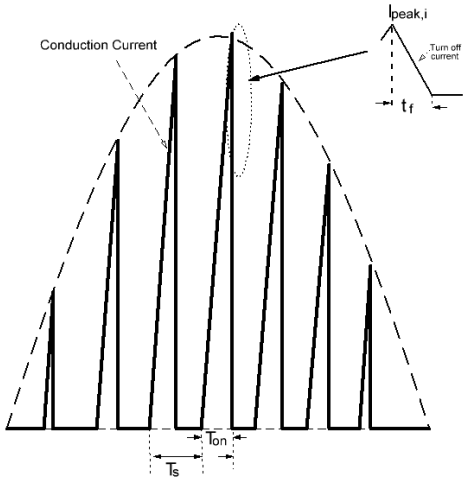


Figure 2: Illustration of current S_1

When (1), (2), and (4) are considered simultaneously, the behavior of the current within S_1 can be described as:

$$I_p(t) = \frac{V}{L_m} t = i_{peak,i} - i_{peak,i}\left(\frac{t - d_i T_s}{t_f}\right) = 0 \quad (6)$$
$$d_i T_s + t_f \le t \le T_s$$

Assuming a MOSFET for switch selection, the voltage at MOSFET S_1 can be defined by:

$$V_{s1}(t) = \left(\frac{V}{L_m} t\right) R_{ds,on} = V_{clamp} - V_{clamp}\left(\frac{d_i T_s + t_f - t}{t_f}\right) = V_{clamp} \quad (7)$$

For the time period spanning from zero to $d_i T_s$, the voltage across the MOSFET is determined by multiplying $R_{ds,on}$ with the current flowing through the device during conduction. Conversely, within the interval from $d_i T_s$ to $d_i T_s + t_f$, the voltage exhibits a linear rise, starting from a value of zero and progressively increasing until it achieves the clamp voltage, V_{clamp}. Subsequently, for all times beyond $d_i T_s + t_f$, the voltage remains consistently fixed at the value of V_{clamp}.

The moment-by-moment power dissipation for switch S_1 can be determined by taking the product of equations (6) and (7), as implemented within the thermal assessment of MOSFET S_1. This analysis is detailed in Section 3.

Operating mode 2: This operational phase initiates upon the deactivation of switch Q_1. The windings' polarity inverts, a consequence of the inability to instantly alter the inductor current, i_p. This event triggers the activation (conduction) of diode D_1. Consequently, the output capacitor charges, concurrently supplying current to the load, R_L. The secondary current, declining linearly, is defined as:

$$i_{se} = I_{se(pk)} - \frac{V_o}{L_s} t \quad (8)$$

Here, L_s symbolizes the magnetizing inductance present within the secondary winding. Within the context of discontinuous conduction mode (DCM), the current flowing through the secondary winding (i_{se}) follows a linear decline, eventually reaching zero before the commencement of the subsequent cycle.

Because the energy transfer occurs solely within the period commencing at 0 and concluding at kT, the input power can be expressed as follows:

$$P_i = \frac{\frac{1}{2L_p I_{p(pk)}^2}}{T} = \frac{(kV_s)^2}{2fL_p} \quad (9)$$

For a given output denoted as n, the resulting output power, indicated as P_o, can be determined via the following methodology:

$$P_o = nP_i = \frac{n(kV_s)^2}{2fL_p} \quad (10)$$

Which can be equated to $P_o = V_0^2/R_L$ to find the output voltage V_o, we employ the following:

$$V_o = V_s k \sqrt{\frac{nR_L}{2fL_p}} \quad (11)$$

Therefore, maintaining a constant V_o is achievable through the stability of the V_s kT product. Since the utmost duty cycle, k_{max}, corresponds to the smallest supply voltage, $V_{s(min)}$, we can determine the permissible k_{max} for the discontinuous mode using:

$$k_{max} = \frac{V_o}{V_{s(\min)}} \sqrt{\frac{2fL_p}{nR_L}} \quad (12)$$

Therefore V_o for k_{max} is then given by the relation

$$V_o = V_{s(\min)} \times k_{max} \sqrt{\frac{nR_L}{2fL_p}} \quad (13)$$

Due to the fact that the collector voltage V_{Q1} of Q_1 achieves its peak when V_s is at its highest value, the formula for determining the maximum collector voltage, $V_{Q1(max)}$, is presented as:

$$V_{Q1(max)} = V_{s(\max)} + \left(\frac{N_p}{N_s}\right) V_o \quad (14)$$

The peak primary current, designated as $I_{p(pk)}$, mirrors the maximum collector current $I_{C(max)}$ of the power switch Q_1, and can be derived using the following formula:

$$I_{C(\max)} = I_{p(pk)} = \frac{2P_L}{kV_s} = \frac{2P_o}{nV_s k} \quad (15)$$

3. Mosfet Thermal Model

The maximum junction temperature, which you'll find detailed in the semiconductor's documentation, plays a vital role in ensuring your circuit's long-term dependability. Exceeding this temperature limit, as explicitly stated by the manufacturer, can lead to irreparable damage to the semiconductor component itself. Conversely, temperature shifts, despite being within acceptable operational limits, can induce mechanical strain within weld seams and connections. Prior research, as cited in, has demonstrated a direct link between the longevity of a MOSFET or MOSFET module and both its average junction temperature, plus the temperature's variances. Thus, for a dependable lifespan assessment, precisely calculating the immediate junction temperature is essential. Within the research realm, the Foster and Cauer thermal models are commonplace when performing such computations. While the transfer function inherent to the Foster model is simpler to integrate, any shift in the thermal environment – for instance, through the inclusion of a heat sink to dissipate heat from the MOSFETs – necessitates recalculation of the resistance/capacitance (R/C) parameters. This specific investigation opts for the Cauer thermal model. It is used alongside the thermal models for the heat sink and buffer layer, illustrated in Figure 3.

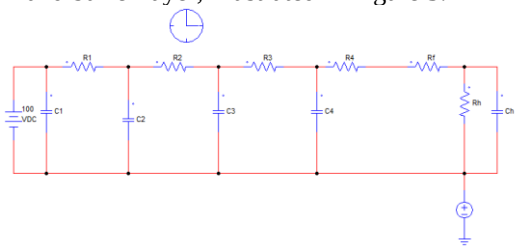


Figure 3: MOSFET and heat sink thermal model. (PSIM).

Within the thermal equivalent circuit, as depicted in Figure 3, the overall losses and the junction temperature of the S_1 MOSFET are simulated correspondingly via the current source labeled I_{loss} and the voltage associated with that current source. The thermal resistances (R_1-R_4) and thermal capacitances (C_1-C_4) are derived from the MOSFET's transient thermal resistance curve, details of which are available within the device's datasheet. Furthermore, the heat sink and insulation layer are represented by R_f, R_h, and C_h. Finally, the ambient temperature functions as the voltage source for the reservoir [1].

4. Mosfet Lifetime Estimation

Previous studies have utilized power cycle tests to gain insights into the durability of semiconductors. During such tests, semiconductor junctions are subjected to both a mean temperature and oscillating temperature variations. Data concerning the longevity of the device, namely the total number and magnitude of these temperature changes leading to breakdown, is gathered to evaluate the component's operational lifespan, based on average temperature parameters. Equation [1], particularly equation (16), produced from this testing, provides a predictive model. This specific formula serves as a basis for predicting the operational life of MOSFETs in this particular analysis.

$$N_f = A \times \Delta T_j^{\alpha} e^{\left(\frac{Q}{RT_m}\right)} \quad (16)$$

Where *A=640, α=-5, Q=7.8*104 Jmol-1*, R is gas constant 8.314 J/mol*K, T_m is the mean temperature and ΔT_j is the peak-to-peak variation in Kelvin. Following a fluctuation in N_f, it is determined that a failure has taken place and the semiconductor's operational duration is over. The importance of counting in projecting lifespan, as detailed later, cannot be overstated. Various counting techniques are documented in the

available resources, encompassing isolevel intersection counting, peak counting, straightforward amplitude/average counting, and rainfall counting. The runoff method is the most widely used technique for measurement. It functions by integrating local minimal and maximal values to define closed contour loops. This approach disregards minor stress cycles, because their impact on overall operational lifespan is considered insignificant. Our research revealed a distinct pattern: the electricity fed into the power grid fluctuates at double the grid's inherent frequency. Furthermore, the semiconductor junction's temperature mirrors this behavior, also exhibiting oscillations at twice the grid's frequency. Consequently, we were able to extract several key parameters using the data in Figure 4. These included precipitation flow counts, network cycle tallies, average temperature readings, and the peak-to-peak variation magnitudes. **[2]**

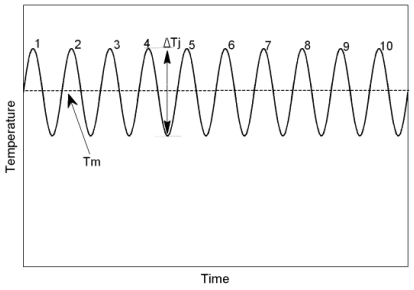


Figure 4: Illustration of the rain count result

5. Simulation Results

A flyback, DCM micro-inverter, designated OST-80 PV, was engineered; its performance characteristics are presented in Table 1. During the simulation, two MOSFET models were chosen for S_1. This decision was predicated on their peak breakdown voltage ratings, current handling capacity, as well as parameters including on-state resistance (R_{ds}), switching thermal resistance (R_{th}) and overall thermal impedance. Lifespan assessments of the MOSFET components were then conducted utilizing the inputs detailed in Table 2 [3].

Table 2: Parameters of the designed DCM flyback micro-inverter.

Parameter	Value
$D_{m,max}$ (18 V)	0.72
Switching frequency, f_s	50 kHz
Turn ratio, n	0.143
Maximum mains voltage, $V_{grid,max}$	325 V ± 15%
Magnetized Induction, L_m	10.52 uH
Input power and voltage	80 W , 18V
voltage MGN, V_m	18 V
MGN current, I_m	4,5 A
Open circuit voltage, V_{oc}	22 V
Short circuit current, I_{sc}	4.9 V
Output voltage/frequency	60 Vrms/50 Hz
switching frequency	62.5 kHz
Output filter L_o/C_o	1.75 mH/330 nF
Transformer winding ratio, n	2
S_1 mosfet	IRFP260
S_2 and S_3 mosfets	IXFK27N80
Diodes D_1& D_2	V30200C

Given the nearly matching DC characteristics of both MOSFETs, we observe a very close resemblance in their total losses. This similarity allows us to focus on the total losses exhibited by a specific MOSFET, the SUU09N10-76P. Figure 5 subsequently depicts these total losses [5], [6].

Table 3: Thermal Parameters.

Parameter	Value SUU09N10-76P	Value IRFI540G
Thermal Parameters		
R_1	979.5767m	152.5307 m
R_2	1.4211	531.4693 m
R_3	463.2464m	1.3026
R_4	1.0192	1.1134
C_1	404.5950u	4.3876 m
C_2	4.4401m	28.8040 m
C_3	47.7255m	120.8742 m
C_3	14.8160m	1.2656
DC parameters		
V_{ds}	100 V	100 V
I_d	9 A	17 A
$R_{ds,on}$	76 mΩ	77 mΩ
R_{th}	3.9 °C/W	3.1 °C/W
Temperature		
R_f, R_h, C_h	0.07°C/W, 4 °C/W, 2 J/°C	

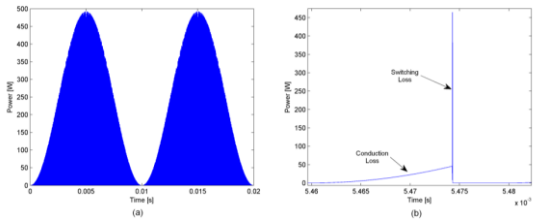


Figure 5: Mosfet power losses for a) one grid period b) one switching cycle.

The thermal transfer function, represented as $T_{junction(s)}/I_{loss(s)}$ and illustrated in Figure 3, has been calculated. Subsequently, the corresponding graphical representations for both MOSFETs are presented in Figure 6. Observing these plots, the thermal equivalent circuit exhibits low-pass filter characteristics, and the switching frequency's effect is multiplicative. Furthermore, analyzing the gain at a frequency of 100 Hz, the IRFI540G shows suppression of the 100 Hz harmonics due to a negative gain. Conversely, the SUU09N10-76P demonstrates an amplification of these same harmonics.

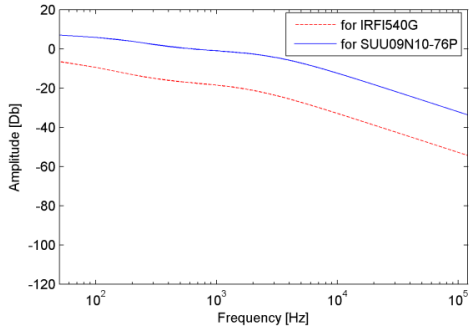


Figure 6: Bode plot for SUU09N10-76P and IRFI540G.

Figure 7 presents a visual depiction of the power loss frequency spectra and the transition temperatures associated with both MOSFET devices. Alongside this, the ambient temperature, symbolized as $T_{ambiant}$, was meticulously recorded, registering a value of 25°C. Subsequently, Figure 8 provides a representation of the MOSFET's instantaneous transition temperature.

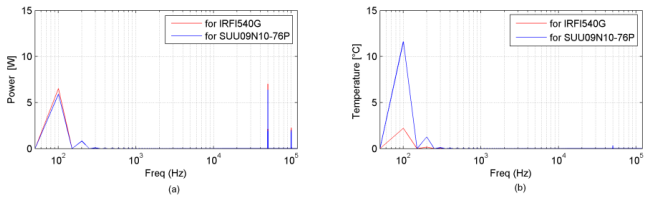


Figure 7 a) Power loss and b) junction temperature frequency spectrum.

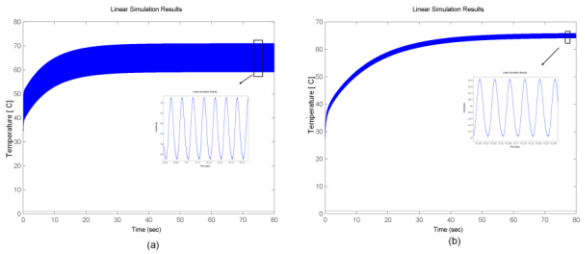


Figure 8: Junction temperature a) SUU09N10-76P and b) IRFI540G.

Peak-to-peak variance alongside mean temperature values for both MOSFET models, operating with an 80 W input, are detailed in Table 3. Employing these figures within equation (8) allows us to determine lifespans: 8100 hours for the SUU09N10-76P, while the IRFI540G reaches 107-108 hours. The IRFI540G boasts an extended lifetime, roughly 13,000 times greater. Consequently, selecting the IRFI540G proves logical when prolonged operational endurance is a critical factor. [5], [6], [7]

Table 3: Thermal simulation results for SUU09N10-76P and IRFI540G at 80 W input Power.

Parameter	Value SUU09N10-76P	Value IRFI540G
ΔT_j	12 °C	1.8 °C
T_m	65 °C	65 °C

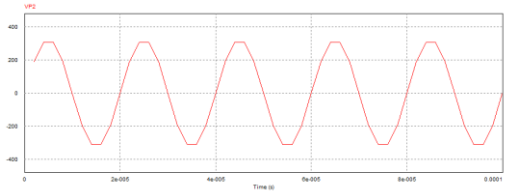


Figure 9: Voltage at the inverter output (PSIM).

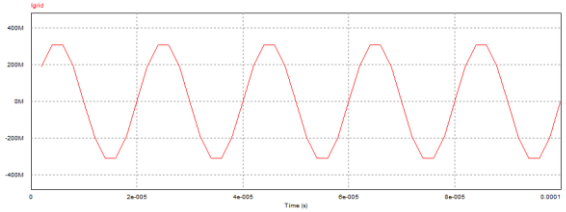


Figure 10: Current intensity at the inverter output (PSIM).

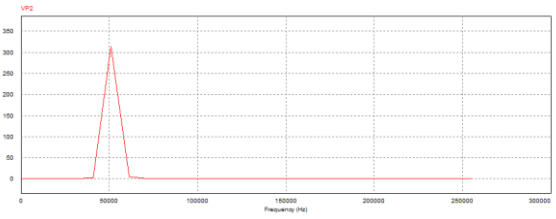


Figure 11: Fast Fourier Transform (FFT) of the transformer output voltage (PSIM).

6. Conclusion

The longevity of S_1 MOSFETs in DCM flyback micro-inverters is compromised by temperature swings occurring at a frequency of 100 Hz, twice the mains frequency. This study focuses on selecting suitable MOSFETs, addressing this limitation. The selection process involves the evaluation of two MOSFETs based on their maximum breakdown voltage, current handling capacity, on-state resistance ($R_{ds,on}$), and thermal resistance (R_{th}). Even though the micro-converter employing DCM flyback design seems to work fine with two MOSFETS, significant variations can be observed in MOSFET lifetime due to the dynamic thermal responses which are part of thermal equivalent circuit. This study suggests that solely considering breakdown voltage, current capacity, $R_{ds,on}$, and R_{th} is insufficient for choosing a dependable MOSFET. Dynamic thermal analysis is also a critical step to guarantee prolonged operational life. [4]

7. Acknowledgment

My special thanks to my professor Stergios Ganatsios and in general to the entire Department of Electrical and Computer Engineering of the University of Western Macedonia. Regarding the author's contribution with this article I hope for the improvement and development of electric vehicles, renewable energy systems, telecommunications equipment and industrial power electronics.

References

1. Y.M Lai, *Power Electronics Handbook*, edited by M.H Rashid, San Diego, CA: Academic Press, 2001, Chapter 20-Power Supplies.
2. J. Hancock, *Application Note AN-CoolMOS-08: SMPS Topologies Overview, Infineon Technologies AG. Munich, Germany, June 2000, www.infineon.com*
3. "Vishay Mosfets." [Online]. Available: http://www.vishay.com/.
4. *High Frequency MOSFET Gate Drivers: Technologies and Applications, ZhiLiang Zhang and Yan-Fei Liu, Institution of Engineering and Technology, 2017*
5. SUU09N10-76P MOSFETs | Vishay
6. IRFI540G pdf, IRFI540G Description, IRFI540G Datasheet, IRFI540G view ::: ALLDATASHEET :::
7. Lifetime Estimation of DCM Flyback Micro inverter, Sinan Zengin and Mutlu Boztepe, Department of Electrical and Electronics Engineering, Ege University 35100 Bornova/ İzmir, 2014 Turkey.

Copyright: *© 2026 Andreas T. This Open Access Article is licensed under a Creative Commons Attribution 4.0 International (CC BY 4.0), which permits unrestricted use, distribution, and reproduction in any medium, provided the original author and source are credited.*